REPORT DOCUMENTATION PAGE

AFRL-SR-AR-TR-05-

0002

1. AGENCY USE ONLY (Leave Blank)	2. REPORT DATE November 10, 2004	3. REPORT TYPE AND DATES COVERED 1 August 2001 – 31 July 2004 FINAL

4. TITLE AND SUBTITLE
Experimental Characterization of Photonic Band Crystals for Tera Hertz Devices

5. FUNDING NUMBERS
F49620-01-1-0484

6. AUTHOR(S)
Dennis W. Prather

7. PERFORMING ORGANIZATION NAME(S) AND ADDRESS(ES)
University of Delaware

8. PERFORMING ORGANIZATION REPORT NUMBER
ELEG332132-103104

9. SPONSORING / MONITORING AGENCY NAME(S) AND ADDRESS(ES)
Air Force Office of Scientific Research
4015 Wilson Boulevard, Room 713
Arlington, VA 22203-1954

10. SPONSORING / MONITORING AGENCY REPORT NUMBER

11. SUPPLEMENTARY NOTES

The views, opinions and/or findings contained in this report are those of the author(s) and should not be construed as an official Department of the Army position, policy or decision, unless so designated by other documentation.

12 a. DISTRIBUTION / AVAILABILITY STATEMENT
Approved for public release: distribution unlimited.

12 b. DISTRIBUTION CODE

13. ABSTRACT (Maximum 200 words)

In this project we are working to develop novel photonic crystal and planar integrated devices for THz frequencies. To achieve these goals we are developing custom high-resolution electron beam lithography (EBL) pattern generation processes and deep reactive etching techniques. To this end we have made progress in the areas of THz device design, fabrication, and characterization and have demonstrated the first THz photonic crystal slab single channel defect waveguide as well as a planar integrated ring cavity coupled waveguide. Details of these devices and the progress made to date in the overall effort are presented in this report.

14. SUBJECT TERMS
THz devices, electron beam lithography, photonic band gap devices, planar integrated THz circuits

15. NUMBER OF PAGES
30

16. PRICE CODE

17. SECURITY CLASSIFICATION OR REPORT	18. SECURITY CLASSIFICATION ON THIS PAGE	19. SECURITY CLASSIFICATION OF ABSTRACT	20. LIMITATION OF ABSTRACT
UNCLASSIFIED	UNCLASSIFIED	UNCLASSIFIED	UL

Table Of Contents

Final Report

The recent emergence of solid-state terahertz sources and detectors have fueled the interest in exploiting THz frequencies, the least tapped region of the electromagnetic spectrum, for their unique science and applications. In fact, THz high-resolution spectroscopy and remote sensing are very active in many fields, such as military, astronomy, Earth, planetary and space science. In addition to other applications, THz wavelengths have advantages for local military communications over other wavelengths in that it is more secure.

However, most THz applications are based on free-space systems, which are bulky and inconvenient. Therefore, to address this problem, we have focused on the simulation, fabrication and characterization of terahertz (THz) micron scale size devices and subsystems in order to realize more compact THz systems. Along these lines, we developed novel photonic crystals, an artificial material that interacts with light in the wavelength scale, to design and fabricate devices such as filters, lens, waveguides, demulitiplexers and THz subsystems. By utilizing currently available IC techniques, we also fabricated and integrated these silicon-based devices. Furthermore, we developed efficient fabrication techniques as well as characterization procedures and systems for these devices, which are now being transferred to AFRL. To this end, this report summarizes the effort, tasks, and milestone achievements in PhC THz device design, analysis and fabrication.

1. Photonic Crystal Filters

As mentioned above, the terahertz (THz) wavelengths provide a unique advantage for secure military communications. Among all of the components, filters play an important role in communication systems, thus sensitive filters would be critical for THz communications. Along this line, we have extensively exploited photonic crystals (PhCs), which have intrinsic frequency selectivity and micron scale size, for constructing micro scale size THz filters. Besides this, we also investigate resonance ring filters. Thus, in this section we demonstrate three kinds of THz filters, namely, guided resonance filters, hybrid lattice PhC filters and ring resonant filters, all of which interact with the terahertz waves on the subwavelength scale.

1.1 Guided Resonant Filter

The guided resonance filter (GRF), consists of a 2D periodic array of air holes that serves to form the PhC structure in high index background material. S. Fan et al, at MIT, intially studied this structure theoretically. It has unique properties that could function as either a narrow band rejection filter or an all-pass transmission filter. The former is very important for channel selection in wavelength-division multiplexing systems. The latter generates significant delay at resonance, while maintaining 100% transmission both on and off resonance. This property, in particular, is useful for applications such as optical delay or dispersion compensation. However, the technical challenge is to fabricate this thin film device and characterized it. Therefore, to address these problems, we proposed a GRF that is based on a silicon-on-insulator (SOI) wafer with the PhC fabricated on the top 2μm thick device layer, shown in Fig. 1. In this case

we do not need to remove the substrate to get the thin film device. Instead we only need to remove the middle 2μm SiO_2 layer, which can be easily done by wet HF etching. Therefore, this device can be easily fabricated using standard e-beam lithography and plasma etching techniques.

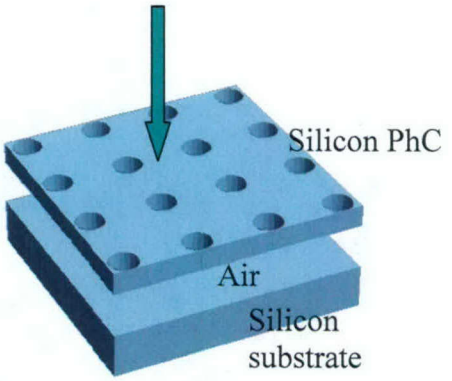

Figure 1. The schematic picture of guided resonance filter and the FDTD simulated transmission spectra of the designed THz guided resonance filter.

The operation mechanism of this filter stems from the guided resonances of the PhCs, which come from the guided modes above the light line, as shown in Fig 2. The light line is defined as the boundary of the gray region, which represents the continuum of radiation modes. For a uniform dielectric slab, these guided modes do not couple into radiation modes because of the underlying continuous transnational symmetry of the structure. However, for the PhC slab, since the presence of the air holes in the crystals lower the translational symmetry of the PhC. These guided modes can couple into radiation modes and possess a finite lifetime. The modes therefore become *guided resonant modes*. To be more specific, when the light is incident to the PhC, there are two possible pathways. The first pathway is a direct transmission process, where a portion of the incident energy goes straight through the slab and generates the initial pulse. The second pathway is an indirect transmission process, where the remaining portion of the incident energy excites the guided resonances. The transmission property, therefore, is determined by the interference between the direct and the indirect pathways. In solid-state and atomic physics, similar interference phenomena are commonly referred to as the Fano resonances. This property has also been exploited in designing of novel photonic-crystal based light-emitting diodes, lasers, and directional output couplers.

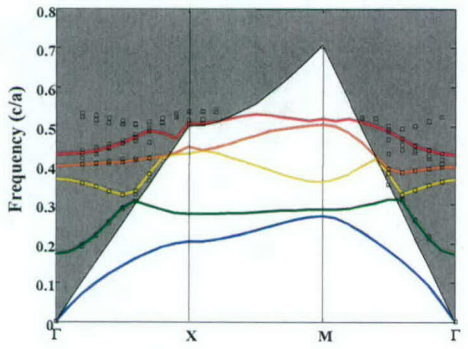

Figure 2 Dispersion diagram of PhC

Using the FDTD method, we excite the resonant modes using a normally incident plane wave pulse. The resulting transmission spectrum is shown in Fig. 3, from the spectrum we notice there are two sharp Lorentzian forms of resonances superimposed upon a smoothly varying background. According to the simulation results, we fabricated a GRF on a SOI wafer with 2 μm device layer, as shown in Fig. 4 (top). The lattice constant a is 3.2μm, with r/a = 0.2. The whole device size is about 600μm × 600μm.

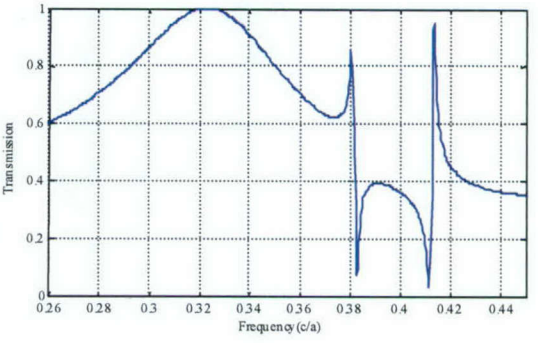

Figure 3. FDTD calculated transmission spectra of GRF.

The fabricated structure was tested with a tunable CO_2 laser (10.2–10.6μm) as a light source, shown in Fig. 4. A thermal camera is positioned directly behind the device to capture the transmitted light. Figure 4 shows snapshots, which were taken by the camera with the wavelength of the incident light varied from 10.2μm to 10.6μm. The circle in the image indicated the GRF and its surrounded silicon area that shined by the CO_2 laser light.

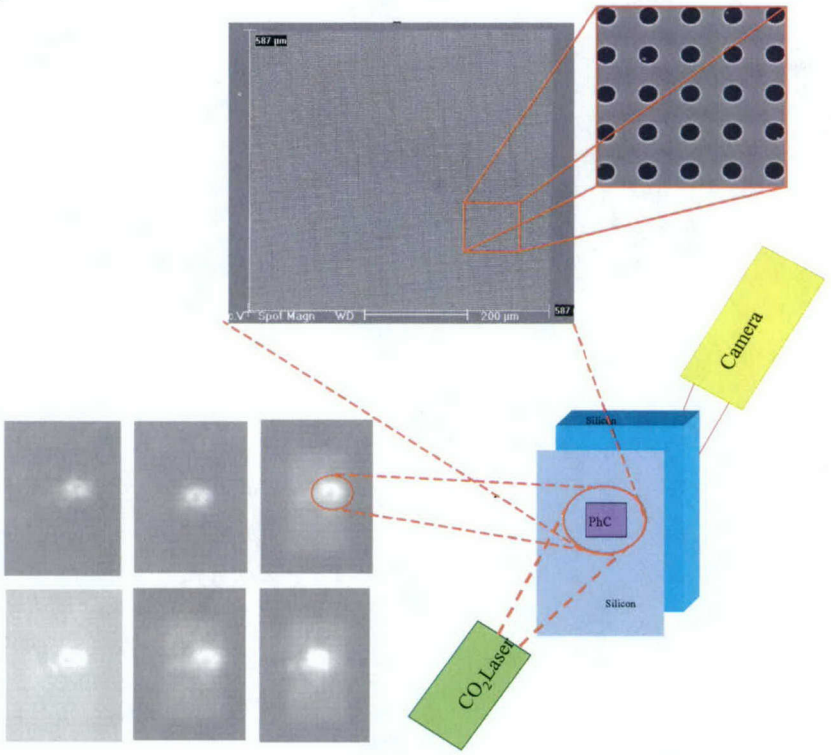

Figure 4. (top), SEM picture of fabricated GRF, the PhC is about 600μm × 600μm, (bottom) pictures obtained by the thermal digital camera, for wavelengths from 10.2- 10.6μm. The circle in the image indicated the GRF and its surrounded silicon area. (right), the schematic setup for the testing of the device.

In the center of the bright spot, which is the GRF, becomes brighter by changing the incident wavlength. This change indicated that the transmission of the GRF is varied with the wavelength changes.

Since the PhC structure is scalable, the same phenomenon should be observed in different wavelength ranges with the PhC perimeters properly scaled. Accordingly, we designed and tested a similar GRF that worked in the microwave regime. Here we present the FDTD simulation and experimental results of the structure as shown in Fig. 5. The simulation result agrees very well with the experimental results in the dropped frequencies of 31.8GHz, 37.0 GHz and 10.7 GHz, however, the drop ratio of the experimental result is greater than FDTD result in the maximum of 60 dB and 15 dB, respectively. Furthermore, there are three-drop peaks in the experiment, which are indicated by the green arrows in Fig. 5, and do not show up in the FDTD simulation. These discrepancies may come from the non-normal incident part of the wave that is emitted by the horn shape waveguide source. From the simulation results, we observe that this oblique incident light results in additional drops in the transmission spectra.

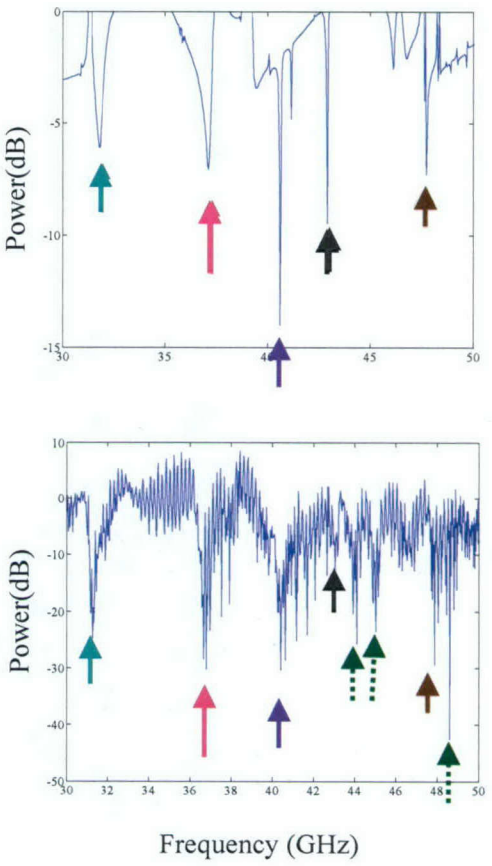

Figure 5. FDTD calculated and experimental measured transmission spectra

Furthermore, using two PhC slabs, we designed a mechanically switchable THz PhC filter with either all-pass transmission or flattop reflection characteristics. This filter is similar to the devices presented by S. Fan et al,

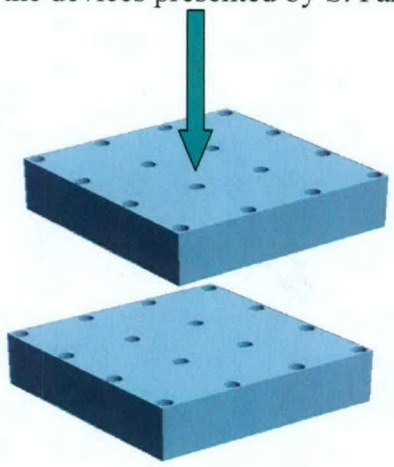

Figure6. Mechanical switchable filter

which consists of two PhC slabs as shown in Fig. 6. Using the FDTD method, we simulated this structure with normally incident light. By simply varying the distance between the slabs as show in Fig. 6., one can switch the transmission characteristic of the structure When the gap between these two slabs is 1.1a, the 0.6947 normalized frequency is dropped from the transmission spectrum, which is fully transmitted when the gap decreases to 0.4a. This filter significantly simplifies signal extraction compared to the same device based on Gires-Tournois interferometers. Furthermore, because of the 90° rotational symmetry of the structure, the spectral response is polarization independent. This reduces the requirement for optical alignment. Furthermore, if we use two SOI wafers instead of

silicon thin film to construct this device, it will simplify the fabrication process, which makes it also easier for integration with other SOI based devices.

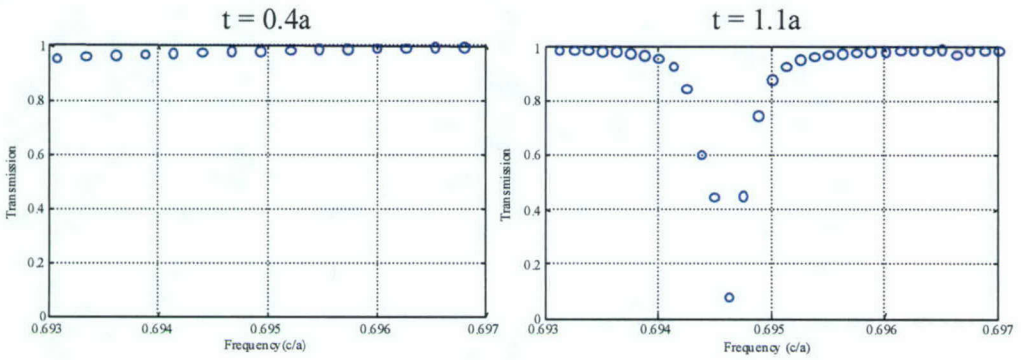

Figure 7. Transmission spectra calculation by FDTD, for the gap between the two PhC slab is t = 0.4a, the wave is 100% transmitted, 0.6947 normalized frequency dropped when the gap increased to 1.1a.

By combining the GRF with other devices, we designed a 3D micro filter system as shown in Fig. 8. Using a two-layer GRF and a layer of ring-resonator structure, we could couple the light into the ring structure at the third layer both vertically and horizontally with the lateral coupling by TIR and vertical coupling by guided resonance. The coupled waves can be fed into a self-collimated waveguide by a ridged waveguide close to the ring. Furthermore, the transmission of this device could be mechanically controlled by adjusting the gap between these slabs. Based on this design, we can build a more complex and multifunctional filter for WDM or other applications.

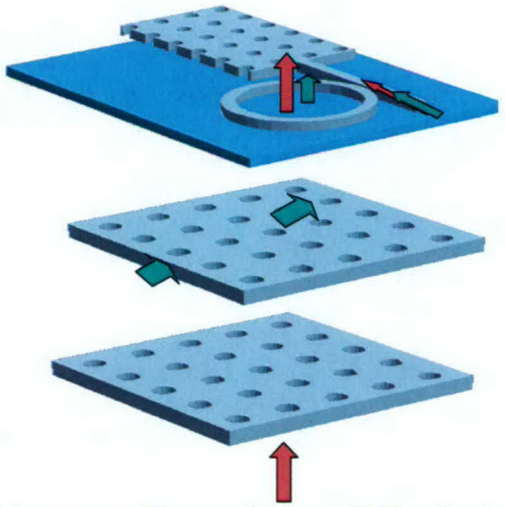

Figure 8. Three-dimensional guided resonance filter, combining a GRF and a ring resonator structures

In addition to the GRF we have also explored the possibility of implementing a hybrid structure PhC dispersion based directional coupler filter presented in the next section.

1.2 Hybrid Structure PhC Directional Coupler Filter

Engineering the dispersion properties of the PhCs gives rise to a new line of devices, such as self-collimated waveguides, superprisms, and negative effective refractive index devices. On the other hand, there are plenty of applications based on their bandgap properties, such as waveguides, cavities, and lasers. If we combine these two special properties together to design devices, there would be great opportunities for us to develop new functional devices and subsystems. Following this line of interest, we designed and experimentally demonstrated a novel hybrid structure PhC directional coupler filter (HPDCF) which utilized these two properties of the PhC. In comparison with ordinary directional couplers, this HPDCF is highly sensitive to frequency varation and easy to integrate with other PhC devices.

To this end, the PhC directional coupler was designed using a hybrid of rectangular and triangular PhC lattice structures. The rectangular lattice served as waveguides, while the triangular lattice functioned as confining boundaries. The schematic structure of the PhC directional coupler is displayed in Fig. 9; the filter layout is completed with a dielectric waveguide and a J-coupler to efficiently couple the light into a PhC waveguide.

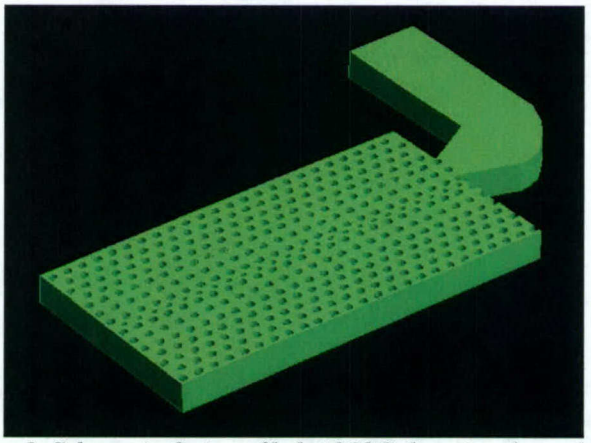

Figure 9. Schematic design of hybrid PhC directional coupler

The PhC directional coupler consists of two rectangular lattice waveguides. Both the rectangular and triangular lattice have the same lattice constant a = 3.125 μm, and r/a = 0.3. They are embedded in the silicon with refractive index of 3.5. The dispersion diagrams of both lattices were computed with PWM as shown in Fig. 10(a) and (b). From the diagrams, we can see most of the second band of the rectangular lattice, which covers the working frequencies of the directional coupler, is in the bandgap of the triangular lattice.

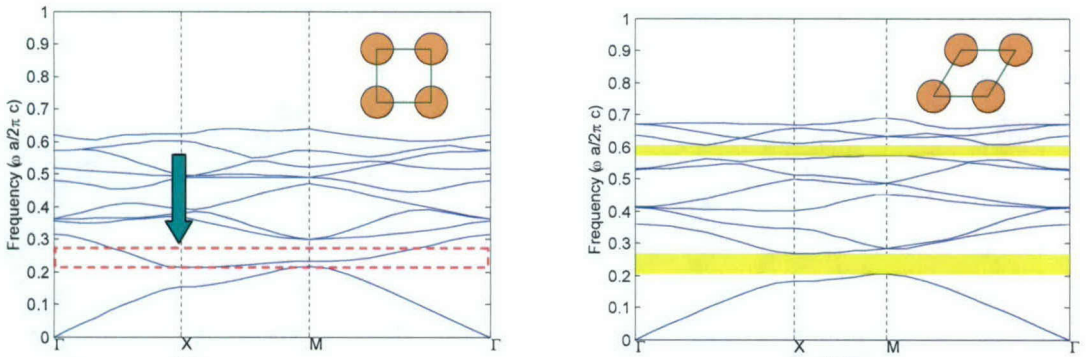

Figure 10. Dispersion diagram calculated by PWM for TE-like polarization, (a) rectangular lattice of air-hole on silicon, (b) triangular lattice of air-hole on silicon. Both of them have the same lattice constant a and r/a ratios. The bandgap of triangular lattice cover most of the second band of the rectangular lattice.

Therefore, light is forbidden to transmit in the triangular lattice resulting in additional confinement in the rectangular waveguides.

The wave propagating and coupling between the rectangular lattice waveguides is determined on their dispersion surfaces, which represent the relationship between frequencies and the associated wave vectors. To better study it, take cross-sections of a dispersion surface at constant frequencies, we obtain Equi-Frequency Contours (EFCs), as shown in Fig. 11(a) and (b) which are calculated by plane-wave method (PWM).The group velocity, v_g, or the direction of light propagation perpendicular to the EFCs, where

$$v_g = \nabla_k \omega\,(k), \tag{1}$$

in which v_g is the group velocity, ω is the frequency and k is the wave vector. This means we can predict the direction of light propagation in a PhC by the shape of the EFCs. Moreover, unlike the ellipsoid shape of ordinary materials, the dispersion surfaces of the photonic crystals is highly dependant on the PhC parameters, such as lattice type, pitch, fill-factor.

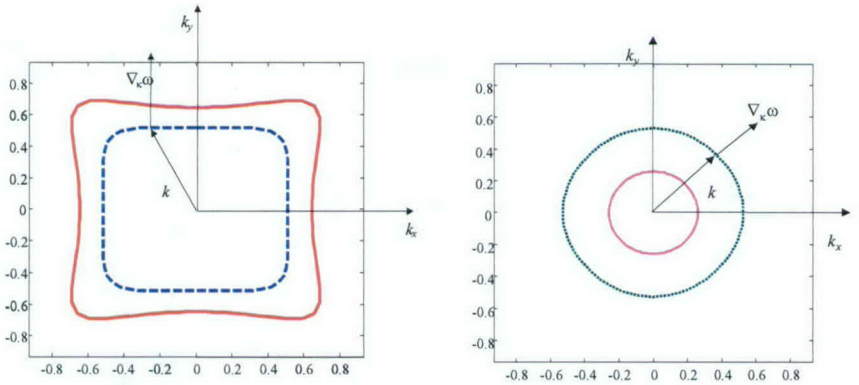

Figure11. EFCs of the rectangular lattice, (a) second band. (b) first band.,

In the case of the circular EFC, which is the same as in the case of homogenous materials, shown in Fig. 11(b), the direction of group velocity is the direction of its phase velocity, which indicates light propagating in it is isotropic. On the other hand, in the square-like EFC case as shown in Fig. 11(a) dashed line, the directions of the group velocity are limited to the two perpendicular directions vertical to its edges. If the light is launched towards one edge of the EFC in a wide range of angles, it is only allowed to propagate in a narrow range of propagating angles, resulting in self-collimation. If the EFC were a perfect square, light would propagate in it without any divergence. However, in reality, it has round corners and non-straight edges that caused the beam divergence. In our designed directional coupler, the coupling between the two PhC waveguides is based on this non-perfectness of the square EFCs. To be more specific, as the light beam is incident into the top waveguide of the directional coupler as shown in Fig. 9, the divergent light is reflected by the boundaries. The resulting evanescent wave, which propagates towards the gap tunnels through the boundaries between them, and then propagates in the bottom waveguide. In this case, any slight variation in the shape of the EFCs can cause different divergent patterns, which, in turn, result in different coupling characteristics. This property distinguishes PhC directional couplers from ordinary couplers.

However, there is a possibility that this device behaves just like an ordinary directional coupler with an effective refractive index. To confirm our analysis that coupling is a function of the dispersion properties of the PhCs, we compared the HPDCF working in the circular EFC region with that working in the square-like EFC region. For the circular EFC, the wave propagated through the PhC in an isotropic-like fashion, as in a uniform media with an effective refractive index. We properly scaled the PhCs to accommodate for the same wavelength propagation in both circular and square-like EFCs.

The steady state results of the FDTD simulation performed at 10.1μm and 10.7μm wavelength of light incident into the HPDCFs are shown in Fig. 12(a) and (b). For the HPDCFs working in the circular EFC region, the coupling characteristic do not change very much when the incident wavelength is varied within the band limits, however, for the coupler working in the second band the coupling changed significantly from coupling to another waveguide to mostly transmitted when the incident wavelength changed from 10.2μm to 10.7μm. Therefore, we can conclude that the dispersion properties are responsible for the couplings. As such the shape of the EFC will highly change the coupling from one channel to the other.

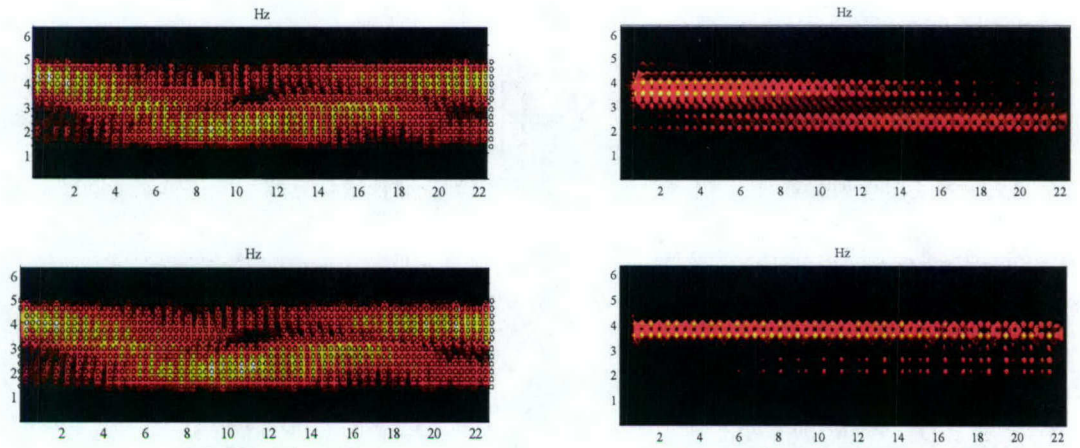

(a) First band (b) Second band

Figure 12.The FDTD simulations of the 10.2μm and 10.7μm light propagated in the HDCs that worked in the first band and second band.

The 3D-FDTD transmission spectra of the light wave transmitted in the two waveguides after transmitted for 40 lattice periods is shown in Fig. 13(a). It agrees well with the steady state results. Based on the initial results attained in the FDTD simulations, we fabricated and tested the HPDCFs, Fig. 13(b) shows SEM picture of a fabricated device (top) and images obtained by the thermal imager (bottom) for the wavelength varied from 10.2μm to 10.6μm. An obvious coupling pattern can be observed from these images. The wave switch from directly transmission to couple into the other waveguide for wavelength changes from 10.2μm to 10.6μm.

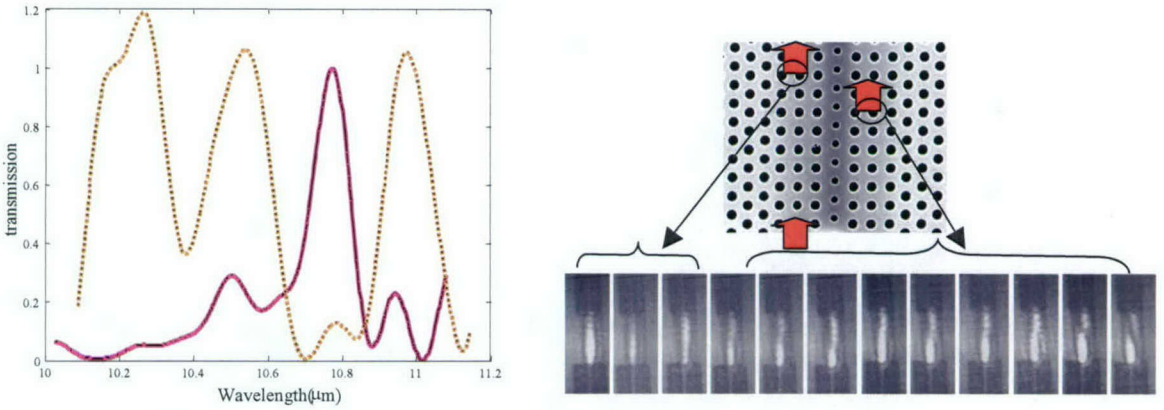

(a) (b)

Figure 13. (a), 3D-FDTD simulation of transmission spectrum of wave in the directional coupler, solid curve represent coupled wave, doted line represent directed transmitted light. (b) SEM picture of fabricated PhC directional coupler (top), and scattered light from the top of the directional coupler obtained by the camera, from left to right the wavelength changed from 10.2μm to 10.6μm.

1.3 THz Ring Cavity Filter

Microring resonators allow for compact channel add-drop filters. They have an important application in add-drop filters ADMs, they are key components for modern networks. Research on ring resonators that have low loss, flat passbands, and a wide free spectral-range (FSR) is intensive. However, not much work have been reported in THz wavelength. In this section, we present our progress in fabricated THz ring cavity filters.

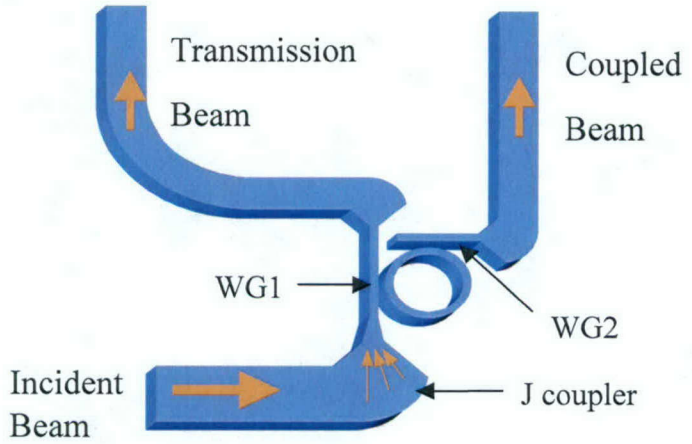

Fig 14. Illustration of a micro-ring coupling planar integrated THz system.

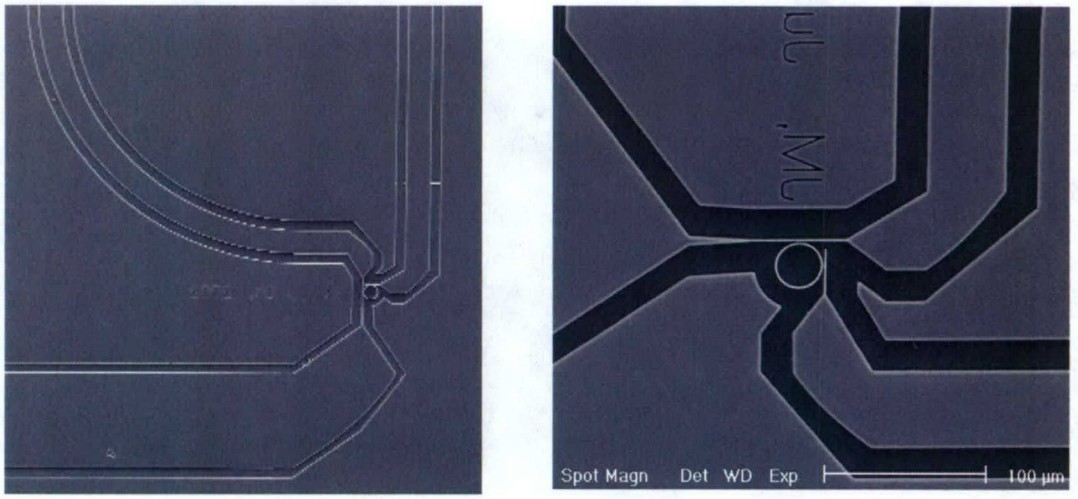

(a) (b)

Fig 15. SEM pictures of an integrated micro-ring planar integrated THz system.

We designed this filter using 2D-and 3D-FDTD methods. Fig. 16(a) shows the spectral response normalized to source spectrum calculated by 2D-FDTD methods. The dashed line represents the spectrum of the beam dropped by ring cavity into the waveguide WG2 and the solid line represents the spectrum of the beam passed through the waveguide WG1. This spectral response shows that there are five resonant frequencies which are 28.2 THz($10.64\mu m$), 29.2 THz($10.27\mu m$), 29.982 THz($10.006\mu m$), 30.9 THz($9.71\mu m$), and 31.8 THz($9.43\mu m$). The average Free Spectral Range (FSR) is about 330nm. The steady-state field distribution of the E_z component at resonant frequency of 29.982 THz is shown in Figure 16 (b), which shows clearly that the light coming from the left port of the horizontal waveguide is totally coupled into the ring and into the out-coupled waveguide.

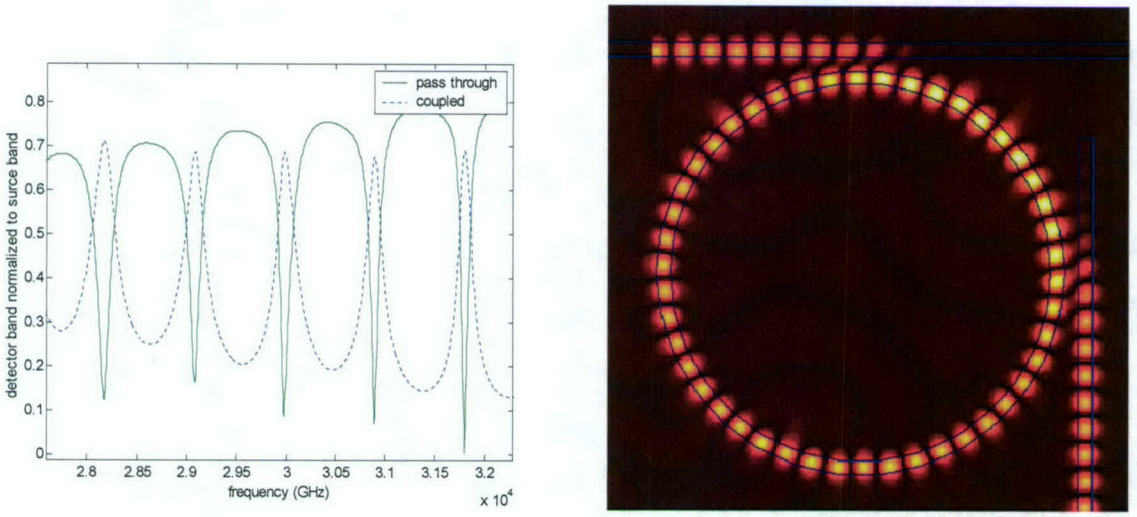

(a) (b)

Fig 16. Calculation of the modes of a ring cavity coupling system: (a) plot of the Free Spectral Range and (B) intensity plot of the electric field component in the ring cavity and coupled waveguides.

To fabricate this device we used $8\mu m$ SOI wafer. The reason for using an SOI is to achieve a high refractive index contrast, which helps to reduce the bending loss and substrate leakage as well as to provide highly confined optical beam in both the waveguide and ring cavity. In the fabrication process we used a chrome on glass mask for UV-lithography to pattern the ring structure. This mask was made at our lab through the process of image reversal and lift-off. To transfer the pattern into the substrate we used a version of the DRIE process. To develop a custom DRIE process for obtaining desired results, we etched the sample using a mixture gas of SF_6 and He in low power and high-pressure condition. Our results indicated that this process worked well when the etch depth is small. However it became worse when the etch depth was increased. The vertical sidewalls became very rough, as shown in Fig. 17 (a). As such we used a variant of the DRIE that alternatively deposit polymer and etching the sample, as shown in Figure 17(b). The later is obviously better than the former.

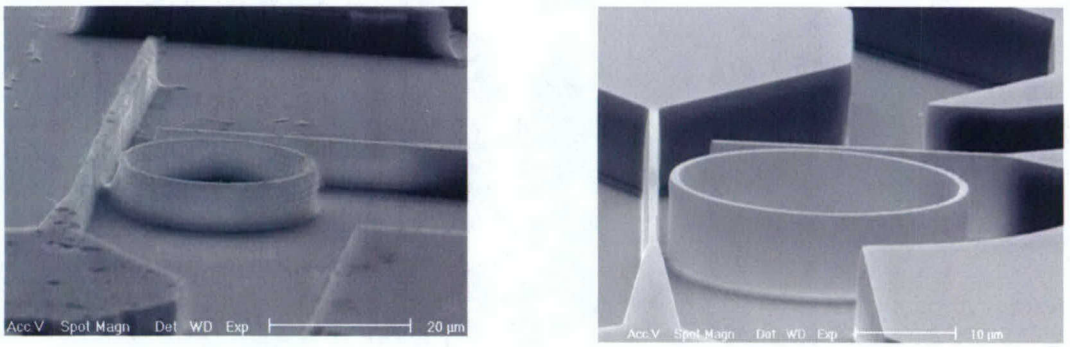

(a) (b)

Fig 17. SEM pictures of an integrated micro-ring planar integrated THz system.

The characterization results are shown in Fig. 18. The light spot in 18(a) is the incident beam. Figure 18(b) shows the scattered light in the ring and the by J-coupler region. The two output light spots can be seen clearly in the Fig 18(c), the left is the light passed through waveguide WG1 and the right is the light coupled into the ring and output waveguide WG2.

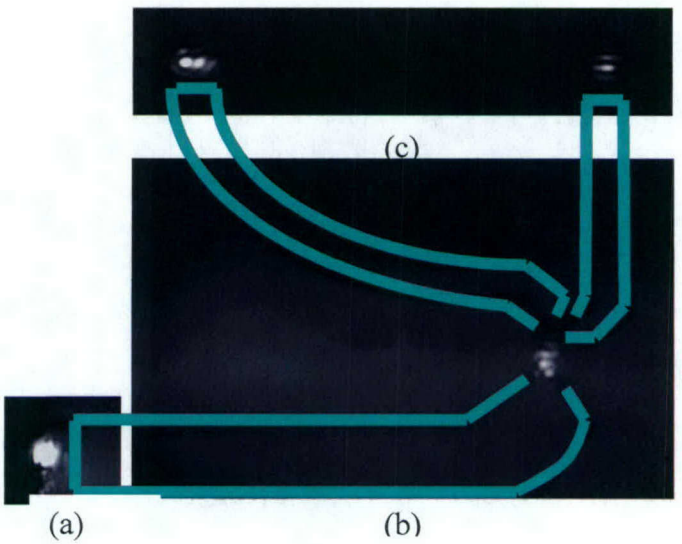

Figure 18. Illustration of the characterized micro-ring cavity coupling system: (a) input beam end fired onto the feed waveguide, (b) light scattered from the focused input waveguide, and (c) out coupled light.

Not only were THz photonic crystal filters and ring cavities examined through the effort of this project but also THz photonic crystal based lenses as discussed in the next section

2. Photonic Crystal Lens

A lens is an essential component for any optical system. However, conventional lenses are limited by their intrinsic diffraction limit. In addition, with the trend of miniaturized systems, a compact lens that could be integrated with other devices is prefered. To this end, two kinds of lenses, namely negative refractive lens and effective refractive index lens are proposed in this project.

2.1. Negative refractive index lens

Artificial materials with a negative value of the refractive index were first analyzed in the late 1960s by V.G.Veselago. Such materials would reverse Snell's law resulting in negative refraction of waves. This artificial material sparked speculation about the potential applications, such as superlens, which suggested that a slab of negative-index material could refocus the rays far better than the diffraction limited conventional positive refractive lens. However, many researchers found the concept of negative refraction and its consequences unsettling.

Recently left hand materials were realized and tested in the microwave regime using combinations of copper rings and wires that were deposited on circuit-board substrates. This new result ignites a renewed interest for exploiting these unusual physical properties. The PhC was confirmed to possess an effective negative refractive index in infrared wavelength region. Up to now, to our knowledge, no related work on terahertz region has been reported. In this report, we presented encouraging results of a THz negative refractive index lens.

Negative index materials also called Left-handed Materials (LHM), exhibit unconventional electromagnetic behavior, which arises from the negative permittivity and permeability thereby leading to negative refraction, hence a negative index material (NIM).The underlying reasons for a PhC to have an effective negative refraction index comes from its special dispersion properties.

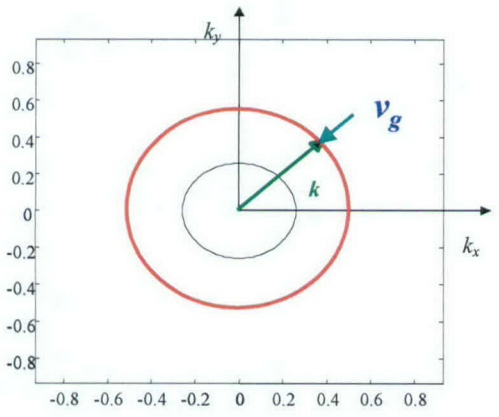

Figure 19. Circular EFC of the PhC

The direction of the group velocity v_g,, is perpendicular to the EFCs. For a circular EFC, the direction of the group velocity is the direction of its radius. If the EFCs move outwards with increasing frequency, then $\boldsymbol{v_g} \cdot \boldsymbol{k} > 0$, as in ordinary materials; however, for PhC the EFCs move inwards with the increasing frequency, $\boldsymbol{v_g} \cdot \boldsymbol{k} < 0$ as shown in Fig. 19. Because the group velocity coincides with the energy velocity, the sign of $\boldsymbol{v_g} \cdot \boldsymbol{k}$ is equivalent to the sign of $\boldsymbol{S} \cdot \boldsymbol{k}$, where **S** is the Poynting vector. So, in accordance with the LHM literature, the sign of the phase refractive index $\mathbf{n_p}$ will be the sign of $\boldsymbol{v_g} \cdot \boldsymbol{k}$. Thus, for PhC the EFC move inwardly with the increasing of the frequency, which means $\boldsymbol{v_g} \cdot \boldsymbol{k} < 0$ or $\mathbf{n_p} < 0$. In

this condition, PhC behaves like a LHM. Following this line, we designed and tested a THz negative refractive index PhC lens (TNRL).

The TNRL is designed in a triangular lattice air-holes on a silicon substrate, which worked in the second band of the PhC for the TM polarized wave, left picture is the dispersion surface of the designed PhC. Figure 20 shows the FDTD simulation of the TM and TE polarized waves incident into the designed TNPL. For TM incident, the light is focused by the PhC, which indicated by the yellow line in the picture and then refocused in the air. On the other hand, for TE polarized light incident, the light is deflected in the PhC without transmission through the PhC.

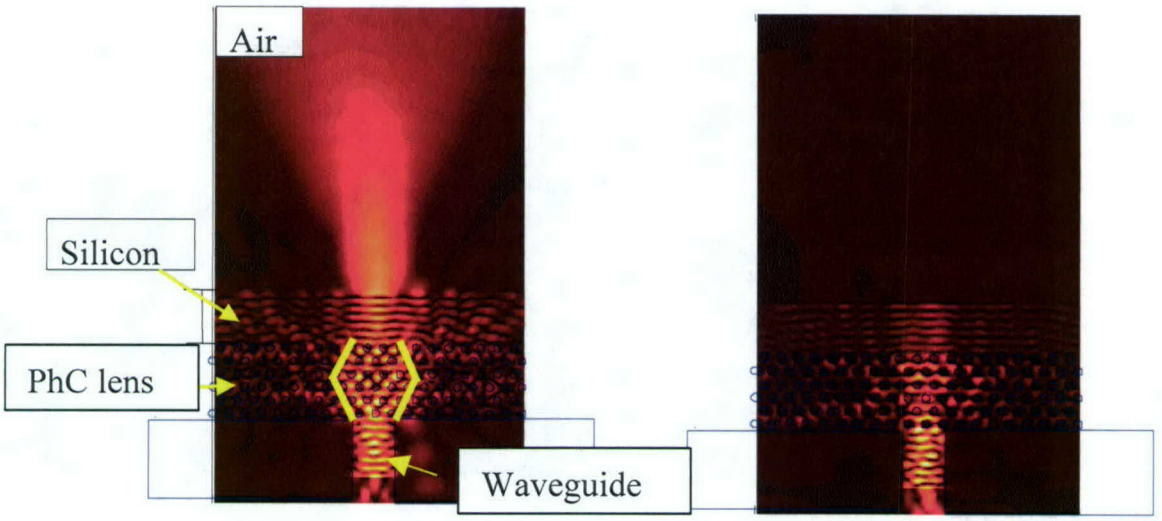

Figure 20. (a) FDTD simulation of designed THz negative refractive index PhC lens (TNRL), the polarization of incident wave is TM polarized. The yellow profile line indicated the focusing in the PhC region because of the nagtive refractive index. (b) The related TE polarized wave incident into the same structure, there is no negative refractive index phenomenon for TE polarized light so the light is not focused.

The reason for these very different behaviors can be analyzed by looking into their Equi-Frequency Contours (EFCs). For the 10.6μm TM polarized light incident, the EFC is almost circular as indicated by the yellow curve in Fig. 21(a).

Therefore, the behavior of the PhC structure is isotropic-like. When the frequency increases, the EFC moves inwardly around the Γ symmetry point, resulting in negative refraction of the beam. For the TE polarized light incident, light propagates in the PhC divergently in the direction perpendicular to its hexagon-like shape EFC as indicated by the thick blue curve in Fig. 21(b).

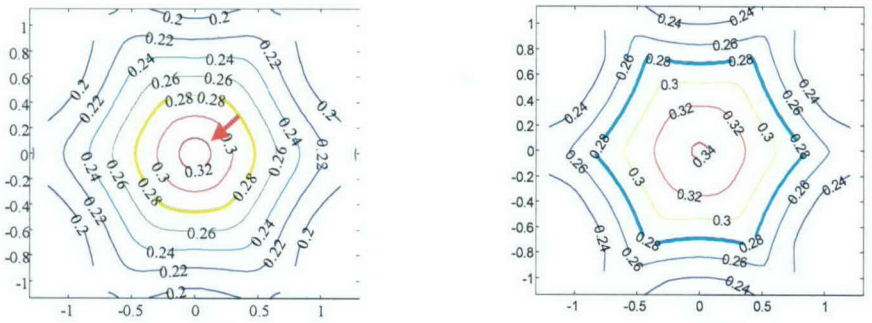

Figure 21. EFCs of the TM polarized light incident (left), the EFC almost circular at the working frequency, which means it behave like an anisotropic material. The arrow indicated with the frequency increase the EFC moves inwardly. According to this, a negative refractive index can be obtained. TE polarized light incident (right), the EFC of the working frequency is not circular, as the thickness line indicated.

To verify this design, we fabricated the designed TNRL on a SOI wafer with device layer of 3μm thickness. The SEM picture of fabricated device is shown in Fig. 22. The PhC lens consists of 6 periods of triangular lattice. The light is first coupled into a wide ridged waveguide of 100 μm wide and then focused by a J-coupler into a narrow waveguide about 10μm. At the other end of the narrow waveguide was the PhC lens. The wide waveguide and the J-coupler are used to increase the coupling efficiency from the CO_2 laser. Figure 22 shows the snap shot of 10.6μm wavelength light incident into the TNRL, a bright focus spot can be observed from the picture. Worthy of mentioning, there is no perceivable reflection at the waveguide lens interface.

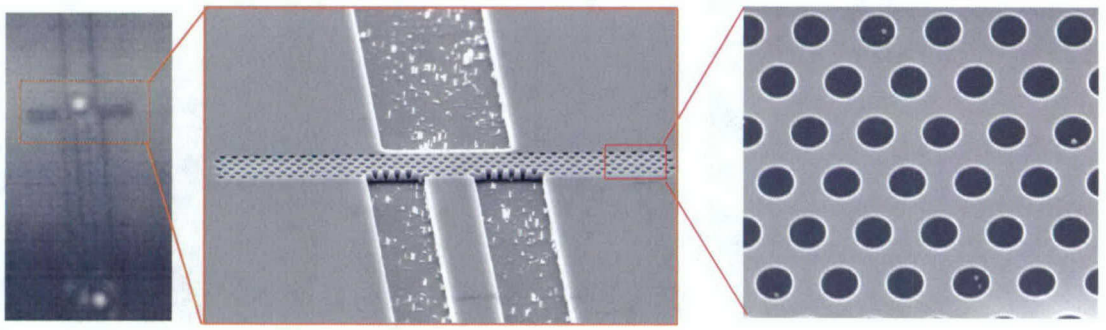

Figure 22. (middle and right) SEM picture of fabricated TNRL on a 3μm thick SOI, (left) snap shot of thermal image of the characterized negative lens.

2.2 Effective Index PhC lens

Most THz applications are based on relatively bulky free space propagation, a compact integrated platform is a favorable choice for more efficient and convenient devices. However, the significant challenge of finding methods to efficiently couple waves into integrated devices remains a challenge. In this section, we propose a very effective coupling structure, THz PhC coupling lens, shown in Fig. 22, which is very compact and can be easily integrated with other devices. Furthermore, in comparison with ordinary silicon lens, the PhC lens is more efficient in that it is based on whole silicon substrate that avoids the coupling losses from silicon-air interfaces. These losses are inevitable in the ordinary silicon lens cases. A 90% coupling efficiency is obtained by 3D FDTD calculations for coupling 10.6μm wave from a 100μm waveguide to a 10μm waveguide. To validate it, the designed device is fabricated, and experimental results show 45% coupling efficiency.

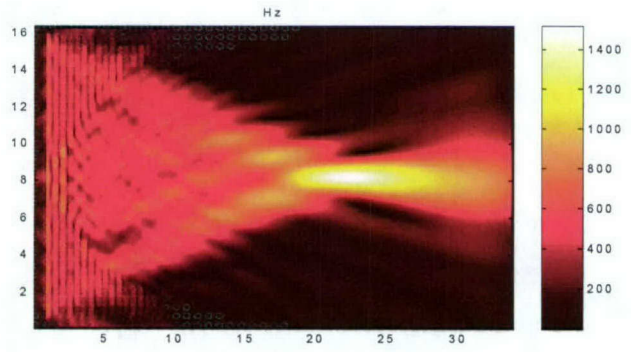

Figure 23. Steady state 3D-FDTD simulation results of the Hz component of the electromagnetic field for the PhC lens at 10.6μm TE polarized Gaussian beam incident.

Using the 2D FDTD and the plane wave method (PWM) algorithms, we designed this PhC lens that consisted of a square lattice of air holes on silicon structure. Figure 24 shows the EFCs at the designed frequency of 10.6μm, the outer line indicates the EFC for the PhC, whereas the inner line represents the EFC of the surrounding free space. Noticed that both of them are circles, which implies that the wave will propagate through the structure according to Snell's law. According to this, we calculated effective refractive index of the PhC. Namely, the ratio of the refractive index of the air and the PhC is equal to the

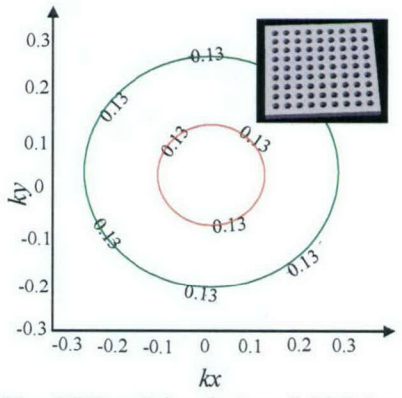

Figure 24. The EFCs of the designed PhC lens and the free space at 10.6μm wavelength, the inner circle represents the EFC of the free space, whereas the outer circle represents the EFC of the PhC, both of them are in the normalized frequency of 0.13(ωa/2πc), where a is the lattice constant

ratio of their radius of the EFCs. With the refractive index of the air =1 and the ratio of their radius equal to 2.34, we obtained the effective refractive index of the PhC, which is 2.34.

We simulated the coupling lens using a 3D-FDTD method as shown in Fig. 23. From these results, a coupling efficiency as high as 90% is achieved by calculating the ratio of the power flow in the waveguide, which is obtained by integrating the energy flow along the direction perpendicular to the wave propagation, and the launched energy flow.

The efficiency of the PhC lens was also experimentally verified by end-firing a focused CO_2 laser light into the coupling structure, in which the PhC lens coupled wave from a 100μm wide waveguide into a 10μm wide waveguide. The resulting coupling efficiency is 45% in the case of 10.6μm wave incident.

An identical but without PhC lens reference structure was fabricated directly adjacent to the waveguide. The left and right images of Fig. 25(a) are taken by the imager show the top view of the devices with the PhC lens and the reference structure, respectively. From it, we can observe a brighter output spot for the PhC lens in comparison to the reference spot, which indicates the efficiency of the PhC lens. It is further proved by the transmission spectra as shown in Fig. 25(b). The blue curve is for the PhC lens, which is much higher than the reference structure, indicated by the purple curve.

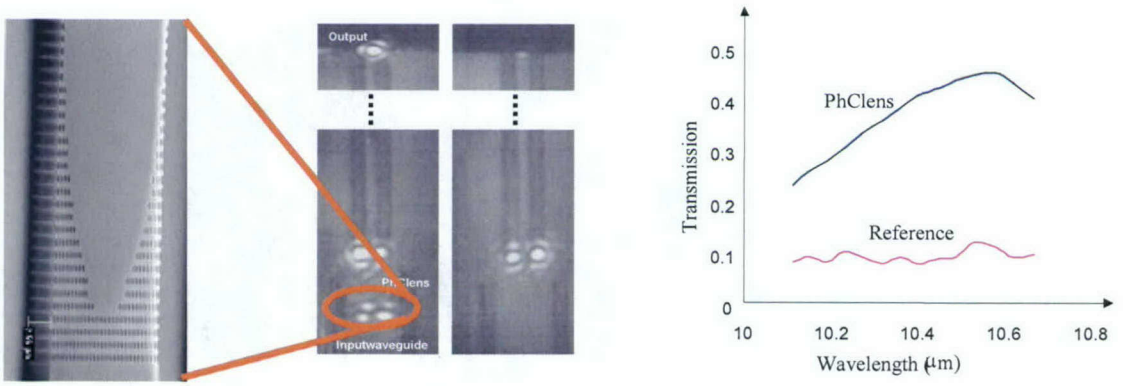

(a) (b)

Figure 25. (a) The Scanning Electrical Microscope (SEM) picture of fabricated PhC lens on a SOI substrate, with device silicon layer of 2.56μm and the images took by the thermal imager with PhC lens coupled 10.6μm wave from a 100 μm waveguide into a 10μm wide dielectric waveguided(left)and the reference structure (right), which is identical to the device but without the PhC lens.e.(b) Measured transmission of PhC lens from 10.1-10.7μm, the highest transmission is 45% at 10.6μm wavelength, and the related transmission of the reference structure, which is flat, highest around 10%.

In the following section we present another technique for vertically coupling THz signals to various devices

3. Prism Coupling THz wave into PhC Waveguides

THz PhC lens has been demonstrated as an efficient coupling structure for integrated circuits. However, the losses that are caused by the mode mismatch between input source and the corresponding two-dimensional (2D) PhC waveguides remains challenging. To solve this problem, we employed a prism coupling method to couple light from a CO_2 laser into a 2D PhC waveguide, which greatly increased the coupling efficiency. According to our calculations, a coupling efficiency as high as 81% can be achieved. In our experimental results we have shown 23% coupling efficiency, to date. Details of this work are presented below.

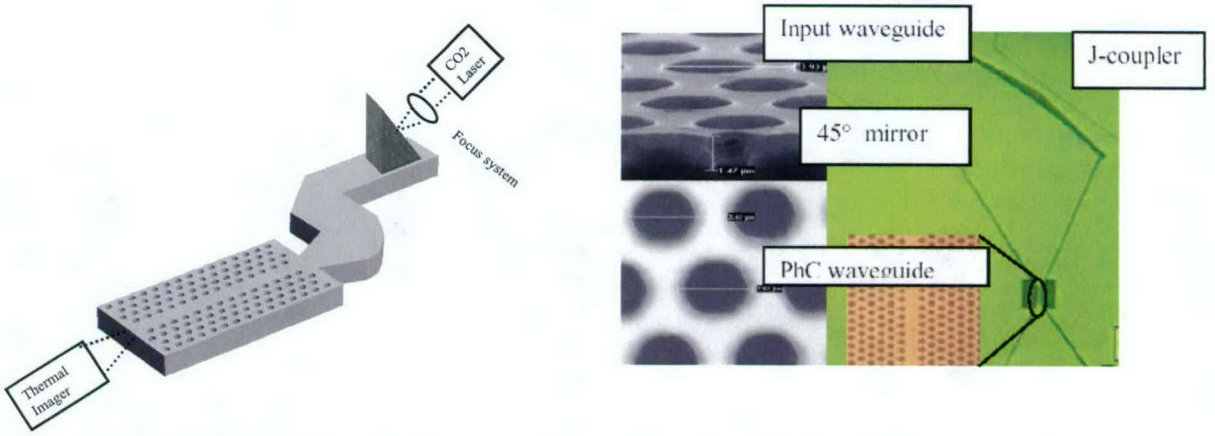

Figure 26. (a), Schematic picture of prism-waveguide coupling setup, CO_2 laser light is focused by a focus system into the right angle of the prism. At the output faucet of the PhCW, a thermal imager that faces it collects the output light.(b),SEM and microscope pictures of a THz PhC waveguide device.

To determine the coupling efficiency experimentally, we fabricated a 2D PhC waveguide on a silicon-on- insulator (SOI) wafer that had a device layer thickness of 2μm. The PhC lattice was designed as a triangular pattern of air holes in silicon as shown in Fig. 26. The air radius, r, over lattice constant, a, was chosen as $r/a = 0.38$, where $a = 3.89\mu m$. In this configuration, the PhC has a bandgap between 9.45μm -12.3μm. The PhC waveguide was created as a line defect by removing one row of air holes in the ΓK direction of the lattice. The device geometry is shown in Fig. 26. Immediately adjacent to the PhC lattice are two tapered ridged waveguides, to help couple the light into and out of the PhC waveguide. Also shown in the figure is a 45° degree mirror and a J-coupler. The J-coupler is an offset parabolic mirror that we use to focus the light from the wide ridged waveguide into the PhC waveguide to further increase the coupling efficiency. The fabricated device is shown in Fig.26.

To demonstrate the high efficiency of prism coupling, we designed and constructed a prism coupling setup, as shown in Fig. 27. In this setup, a TE polarized tunable CO_2 laser (10.6μm) beam is focused to a spot-size of about 100μm, on the hypotenuse of a 90° silicon prism (refractive index 3.42). The prism is mounted on a *xyz* micromanipulator stage. Opposite the stage is the PhC waveguide taped on the head of a pneumatic plunger.

The distance between the prism and the waveguide is adjusted by changing the pressure on the pneumatic plunger. To allow for maximum freedom of adjustment, the waveguide and the prism are mounted on a rotation stage together on a *xyz* translation stage. A thermal image with a reflective objective located in front of it is placed facing the output end of the waveguide to observe the output coupled light. The imager and the laser light source are all mounted on the *xyz* translation stage to achieve precise alignment. By optimizing the incident angle on the prism's hypotenuse, the prism-waveguide separation distance, the width of incident beam, and the position of the incident light on the prism, we were able to obtain optimized coupling. With the incident angle and airgap thickness optimized, the highest coupling occurs when the light is directly incident to the right angle of the prism. The reason for this is that if the incident wave was too far to the right or left of the right angle, some of the incident power will be either reflected or transmitted directly into the waveguide instead of entering the prism.

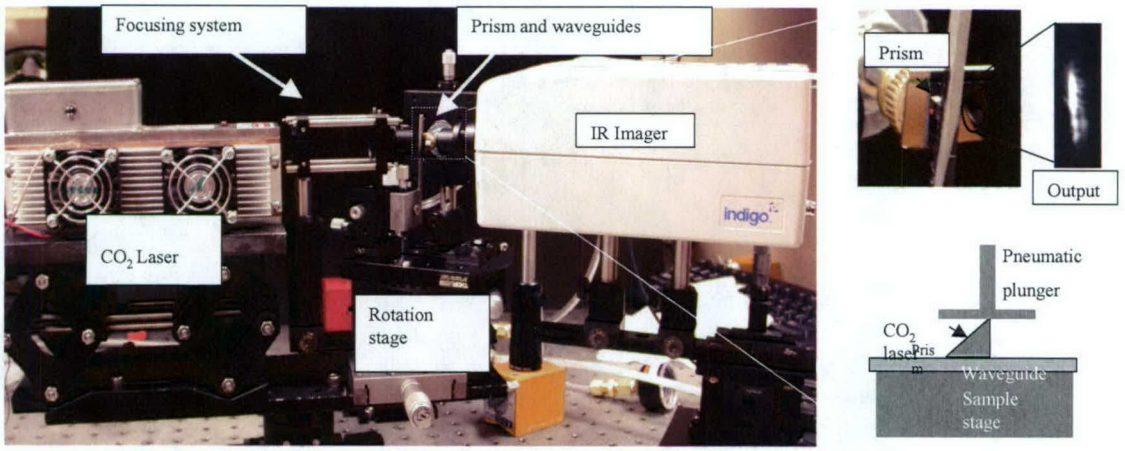

Figure 27. Picture of optical setup for prism coupling light into THz PhC waveguides, a CO_2 laser is used as light source to incident into prism, which is tightly pressed to the waveguide device. The output light from the waveguide are collected by a IR thermal imager. the right picture is the zoom in image of the prism coupling and output light obtained by the thermal imager.

To verify this, we used a 2D-FDTD method to simulate light incident in the prism at different positions. Figure 28 (a), (b) and (c) show the wave incident into the prism at the

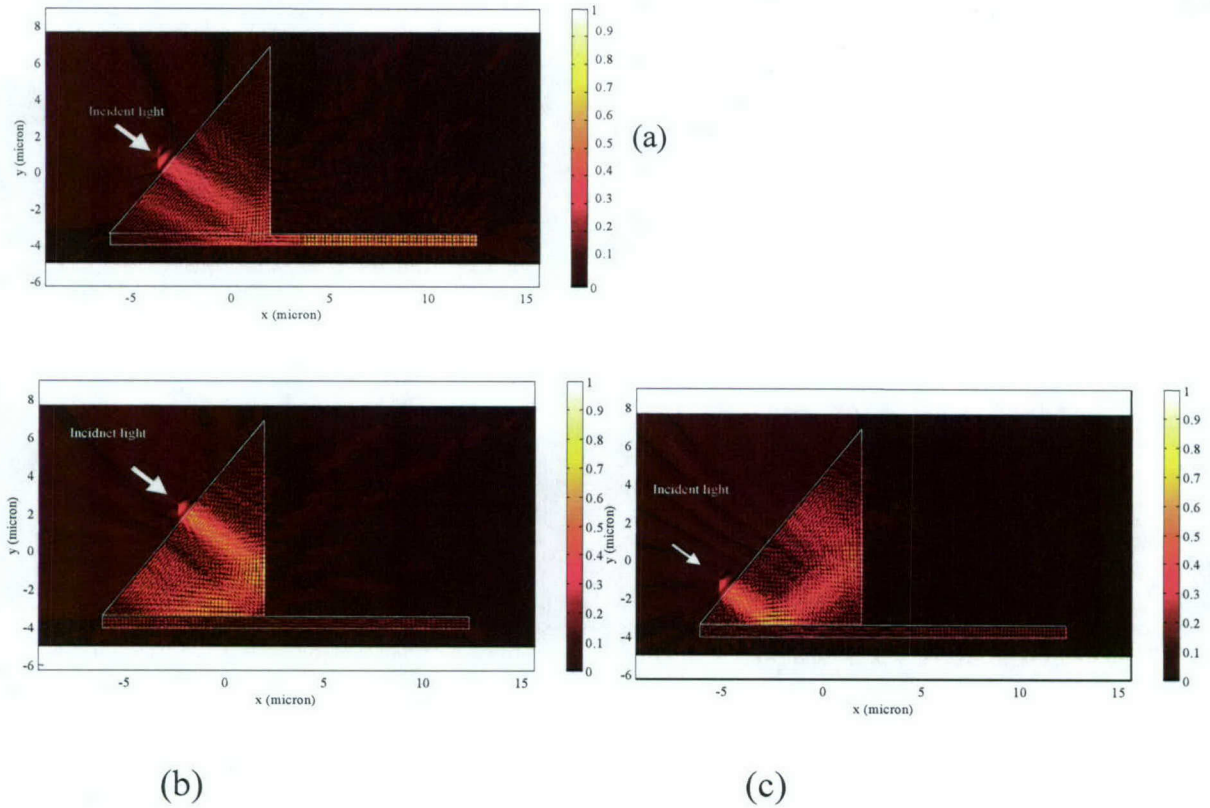

Figure 28. Steady state 2D-FDTD simulations of light incidents, (a) to the right angle of the prism, (b) to the left of the right angle of the prism, and(C) to the right of the right angle of the prism. From the simulation, it can be clearly seen that only the light incident to the right angle of the prism that realized the best coupling efficiency as shown in (a), in the cases of to the left or right of the right angle, the light is reflected back to the prism.

right angle of the prism, to the left, and to the right of the right angle, respectively. In Fig. 28(a), light coupled to the waveguide from the prism without significant reflection from the prism-waveguide interface, indicates an efficient power transfer. In the case of Fig. 28(b) and (c), almost all the light reflected back to the prism with just a very small portion of the wave coupled to the waveguide. These simulation results confirmed the notions above.

To this end, we demonstrated the first ever observed 10.6μm light prism coupled into a PhC waveguide. Our measured coupling efficiency was 23%, which was obtained for TE polarized light. From both of our theoretical and experimental results, we found prism coupling is indeed a very efficient way to couple light into subwavelength waveguides. Furthermore, we compared the prism coupling to the other coupling methods, such as end-fire and grating couplings, and it was confirmed that prism coupling is much more efficient than the other methods.

4. Prism fiber PhC 3D DWDM

Prism coupling was confirmed in the last section to be an efficient method to couple light into and out of planar THz circuits. Based on this, we designed a Dense Wavelength Division Multiplexing (DWDM) device using a combination of prism, fiber and PhC cavities, which is a potential way to increase the capacity of transmission bandwidth in communication systems. Existing DWDM systems, such as grating based DWDMs, Fabry-Perot DWDMs, and arrayed waveguide grating systems tend to be quite large, having a size ranging from several millimeters to several centimeters. For this reason a PhC device offers a significant advantaged, because of its sub wavelength scale size and ease of integration with the other devices. Therefore, we designed and fabricated a PhC 3D-DWDM based on the use of PhC cavities. To this end, a PhC cavity is formed using a point defect in an otherwise perfect photonic crystal lattice. As a result, a localized mode (or group of modes) may be found at frequencies within the PBG. In this way, the point defect acts as a resonant cavity. In our design, the photonic crystal cavities are formed by point defects in a triangle lattice of air holes in silicon.

By manipulating the parameters of air holes, a resonant cavity can be obtained. We designed the cavities in such a way that when a broadband light source impinges it, certain frequencies will resonate in specific cavities and then couple out through their associated waveguides, which are close to them. In this way, we realize DWDM device. For some applications, we may also need to couple the light into adjacent vertical layers, so we designed a 3D-DWDM system, as shown in Fig. 29. In this device, we coupled light into a wide, or feed, waveguide using our prism coupling approach. Next it was reflected by a 45° angle mirror into a J-coupler.

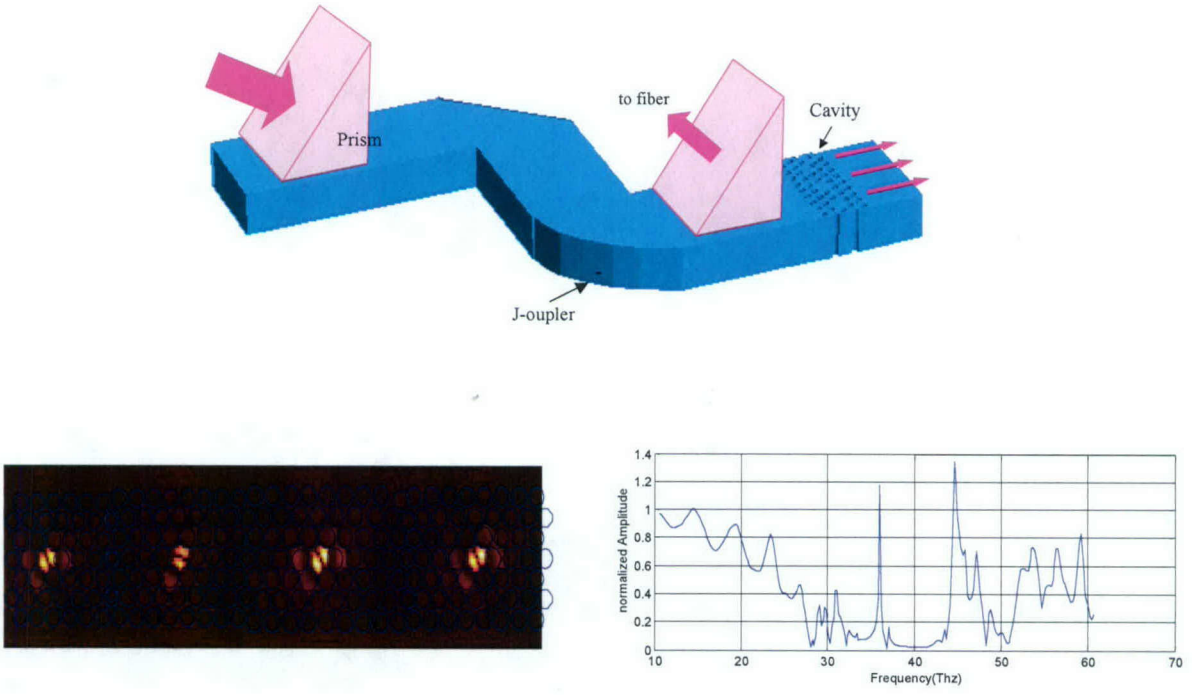

Figure 29. Schematic picture of designed prism to fiber 3D DWDM structure, 2D-FDTD simulation results of the designed WDM.

The J-coupler focused the light into the cavities that constituted the 2D-DWDM then dropped the desired frequencies to the waveguide close to them. The reflected light by the PhC coupled out of the device by another identical prism, which is put on top of the feed waveguide. At this point, the light is coupled to another layer by a fiber that is connected to another prism. In this way, a 3D-DWDM is realized. Figure 29 shows transmission spectra of the light coupled out of one of the cavities and the 2D-FDTD steady state simulation results of a broadband THz pulse incident onto the device. From the transmission spectra, we can see that a very narrow peak is coupled out of one of the cavity to the waveguide. From the steady state result we can see the light, indeed, resonated within the cavities.

One of the advantages of the PhCs is that they are scaleable, the same phenomenon could be observed in different frequencies, if we properly designed the parameters. Therefore, we present the results obtained in infrared wavelength. Figure 30 shows the fabricated 3D-DWDM devices on an SOI wafer.

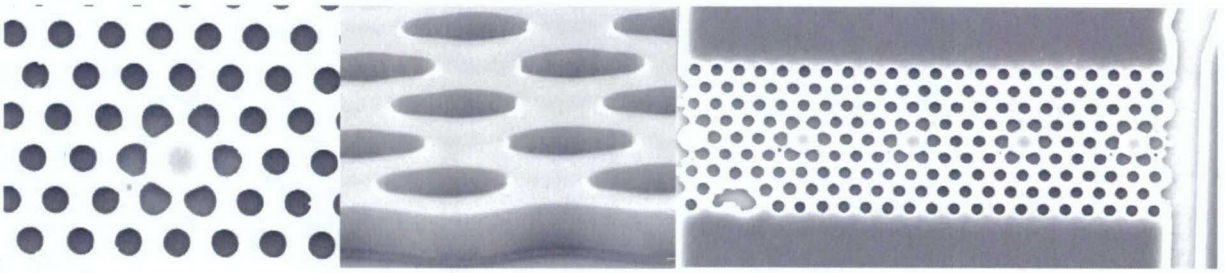

Fig. 30. SEM pictures of fabricated PhC cavity structures. r/a=0.35, a=3.9μm, defects diameter d= 3.2 μm, device thickness=2 μm.

Figure 31 shows the 3D-FDTD simulation results using our SEMFDTD software. Which directly used SEM picture of fabricated device shown in Fig. 32 as the input structure. Therefore, the simulated results would be expected to be closer to the experimental results, which was observed.

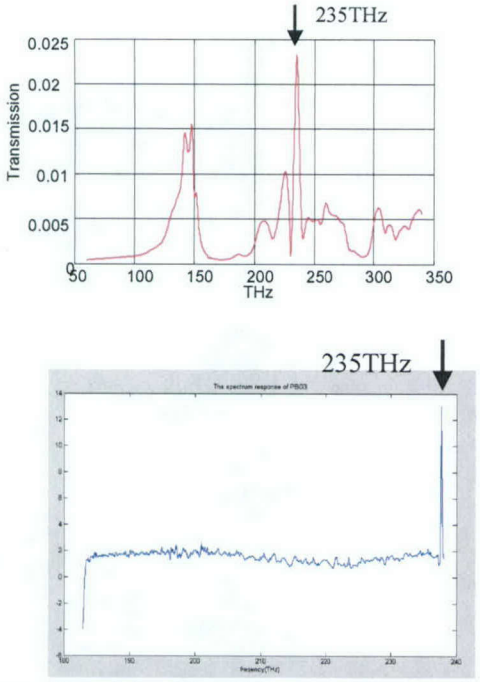

Figure 31. (a), 3D-FDTD simulation of TE polarized wave incident into the PhC cavity filter, (b) experimental results of characterized PhC cavity filter

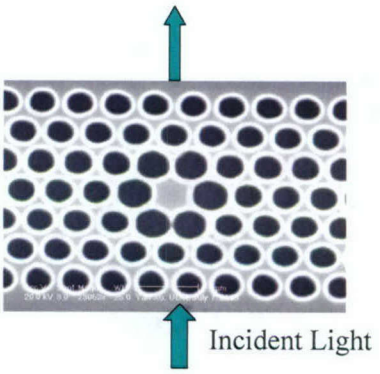

Figure 32.Fabricated PhC cavity, which is used for SEMFDTD simulations

5. THz Waveguides

DWDM, filters, and lens are important functional devices for THz applications. In order to interconnect these devices, an important element is needed. A linear waveguide is needed to carry light to and from those components. In this section, we introduce two types of waveguides that have potential for THz applications, namely, self-collimated waveguides, and line-defect waveguides.

5.1 Self-collimated Waveguides

In keeping with the near universal trend of miniaturization, ultra-small size THz devices may help to improve performance and thereby become important components in emerging THz technologies. Recent progress in self-collimation phenomenon in PhCs has spurred new interest in the development of a new means for low loss waveguides that offer structureless confinement of light in the infrared region. To the best of our knowledge, no related work has been reported in the THz wavelength region for the

demonstration of both guiding and very low loss THz self-collimated waveguides. Therefore, in this report we present such devices where using a tunable CO_2 laser as a source we observe 2.56dB/mm propagation loss in our self-collimated waveguide fabricated on SOI. 3D-FDTD calculated transmission spectra agree very well with the measured results at the peak wavelength of 10.5μm.

Figure 33 shows a device which was fabricated in a silicon-on–insulator (SOI) wafer with the silicon device layer thickness of 2μm. In between the two ridged waveguides is a PhC that contains an array of rectangular air holes with a lattice constant, a = 3.1μm, and an air-hole radius r over a, r/a = 0.3.

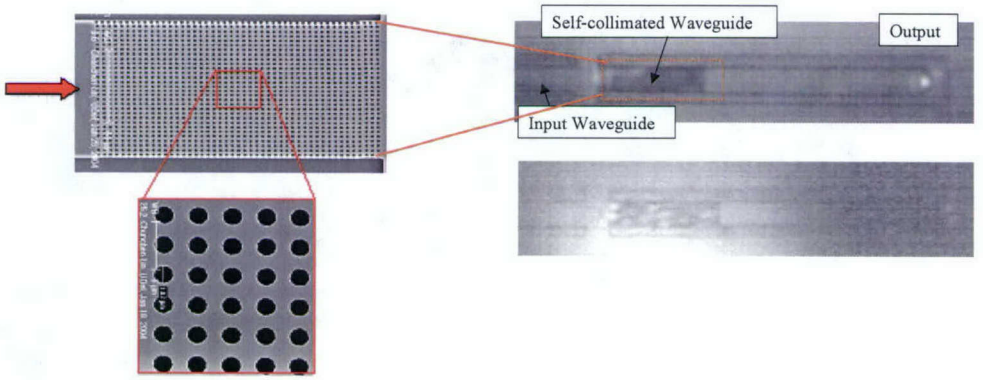

Figure 33. SEM picture of self-collimated waveguide, with a total length of160μm, and a width of 100μm. Lattice period a = 3.123μm, r/a = 0.3. The top view of the self-collimated waveguide that obtained by camera, upper, at 10.5μm wavelength, there is no significant scattering in the PhC region, an output spot can be observed, lower, at 10.1μm wavelength, a bright scattering spot can be seen from the top of the output facet,

Figure 33 (left) shows beam propagation along the self-collimation waveguide for wavelengths 10.1 μm to 10.5 μm. The top view image of the PhC and the output waveguide edges are obtained by the camera. From the picture, an output spot can be observed for the 10.5μm wave (upper picture). It is worth to mentioning that there is no perceived presence of strong scattering on the top of the PhC region, which is typical in conventional line-defect waveguides and is indicative of very good vertical confinement in the PhC guiding region. However, there is very strong scattering from the PhC region for the 10.1μm wave, and the output light is very weak. (lower picture). These results suggest 10.1μm wavelength light, unlike 10.5μm light, is not as well confined in the vertical direction.

To analyze these results, a 3D-FDTD scheme is used to simulate wave propagation in the PhC waveguide, as shown in Fig. 34. In the case of the 10.5μm wave, very good waveguiding can be observed, which indicates that the wave propagation in the PhC is self-collimated. On the other hand, for the 10.1μm incident, the wave is wideband and decays along the propagation direction. As such, the 3D-FDTD simulation results are consistent with the experimental results mentioned above.

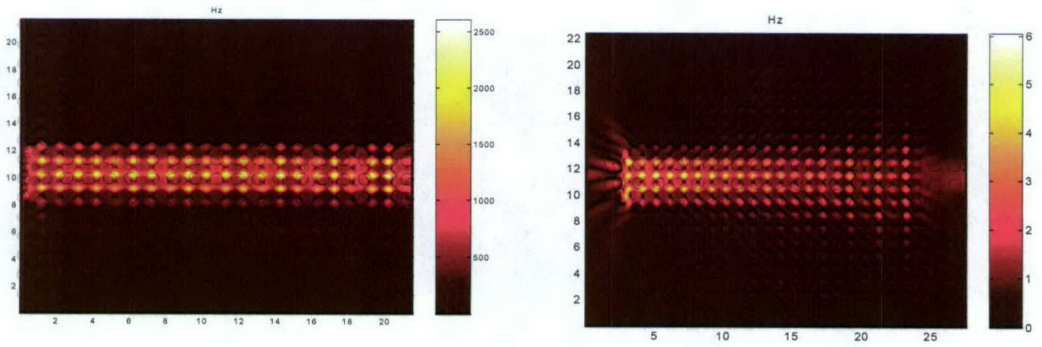

Figure 34. 3D-FDTD simulation of 10.5μm (top), and 10.1μm (bottom) wave propagating in the PhC. At 10.5μm, very good confine propagation can be observed, whereas at 10.1μm, the transmission is decreased significantly with the propagation length.

To evaluate the transmission efficiency in the self-collimation waveguide, we measured the transmission loss using the cutback method. From the measurement, we determined a propagation loss as low as 2.56 dB/mm. This loss can be decreased by designing a graded interface between the ridged waveguide and the PhC waveguide to eliminate the loss caused by Fresnel reflections between the input facet and the waveguide PhC interface, as well as the output facet and PhC waveguide interface

5.2 THz PhC Line-Defect Waveguides

Photonic crystal waveguides are formed by a line defects in PhCs that produces waveguide modes within the photonic bandgap. These modes, guided by the band gap of the bulk crystal, can exhibit near-zero reflection and loss through straight waveguides and sharp bends, which are expected to lead to ultrasmall lightwave integrated circuits. Although theoretical, experimental studies of photonic crystal waveguides within the optical wavelength region have been reported, none of these present waveguides in the THz wave regime.

To this end, we present a THz wave-propagation and transmittance study of Two-dimensional (2D) photonic crystal waveguides, which are formed by single channel defects in the photonic crystal (PhC) lattice which based on a silicon-on-isolator (SOI) wafer. The fabricated structure is shown in Fig. 35

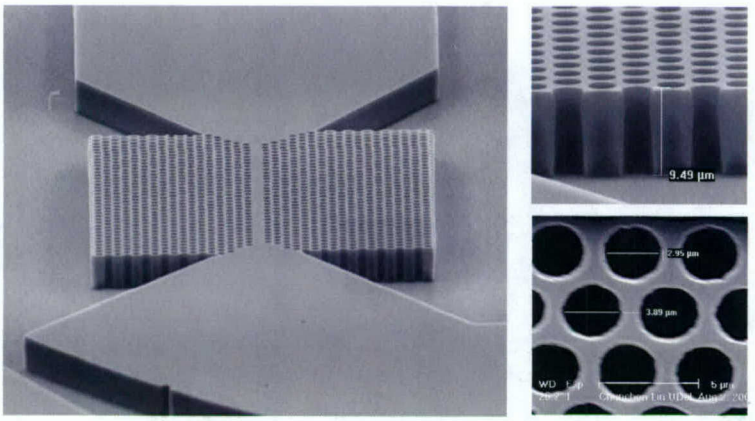

Figure 35.(Left) SEM picture of PhC waveguide, the total length of it is 160µm, and the width of it is 100µm. (right) SEM pictures of side view and top view of the PhC Waveguide, the thickness of it is 9.49 µm, the lattice constant a = 3.89 µm, and the hole diameter is 2.95 µm.

The setup for optical characterization is shown in Fig. 36. The laser light was tightly focused into the dielectric waveguide by a 0.5"-focal length focusing lens. The light was then focused by the J-coupler into the PhC waveguide, and the output light was collected and imaged by a reflecting microscope objective onto a pyroelectric thermal detector array (Electrophysics PV-320). The thermal imager was also employed to obtain optimal optical alignment, to monitor the scattering of the light from the top, as well as to view the output light from the output waveguide. This was accomplished in site by the use of a gold-coated mirror mounted above the sample at a 45-degree angle mirror, which provided a top-down view for the camera.

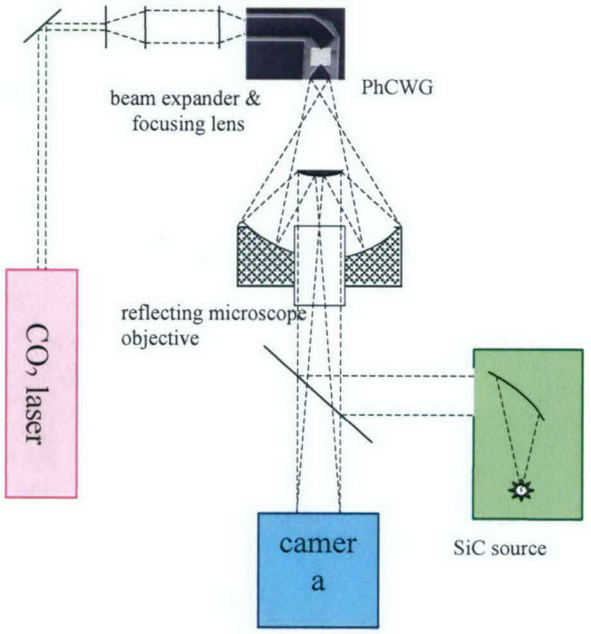

Figure 36. Schematic layout of the optical setup for measuring transmittance spectra and optical propagation.

A broadband-emitting silicon carbide filament was used to illuminate the sample through a beam splitter to image the sample and to facilitate the alignment of the end-fire coupled input. Figure 37 shows the image obtained by the thermal camera with CO_2 laser light incident on the waveguide

The input and output facets were polished to get a better coupling result. The left and right upper images are the top view of the input facet, the J-coupler, and PhC waveguides, respectively. The lower photo is the image of the output light.From the top view of the sample, we observe that vertical out-of-plane losses from the PhC waveguide were not detectable; this indicates good vertical confinement within the PhC waveguide. The output picture, which is in the lower right of Fig. 37, was obtained by positioning the IR camera directly facing the output faucet. The output light can be clearly seen from the picture.

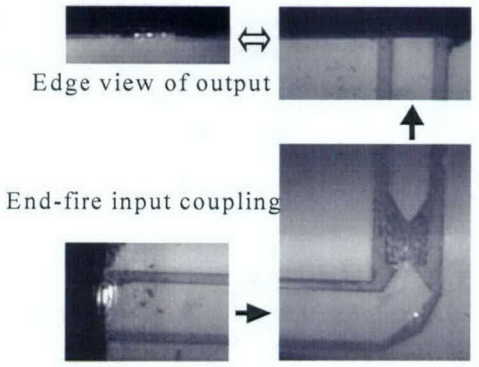

Figure 37. Image acquired by thermal imager, (left upper) upper view of the output facet, (right upper) topview of the output facet, (lower left) top view of the input facet, (lower right) top view of the 2D-PhC waveguide.

6. Conclusion

In this report, we have summarized our 3 years effort in developing and demonstrating photonic crystal devices. Devices and subsystems that bear the most recent progress in the field have been presented, such as filter, lens, WDM, waveguides and subsystems that are based on them. Many of them are presented for the first time, to the best of our knowledge. In addition, efficient micro fabrication procedures and testing systems were developed in our lab. Using our customized simulation software, we designed THz devices and subsystems and then fabricated and tested them in our lab.

MASTER COPY: PLEASE KEEP THIS "MEMORANDUM OF TRANSMITTAL" BLANK FOR REPRODUCTION PURPOSES. WHEN REPORTS ARE GENERATED UNDER THE ARO SPONSORSHIP, FORWARD A COMPLETED COPY OF THIS FORM WITH EACH REPORT SHIPMENT TO THE ARO. THIS WILL ASSURE PROPER IDENTIFICATION. NOT TO BE USED FOR INTERIM PROGRESS REPORTS; SEE PAGE 2 FOR INTERIM PROGRESS REPORT INSTRUCTIONS.

MEMORANDUM OF TRANSMITTAL

Air Force Office of Scientific Research
ATTN: Dr. Gernot Pomrenke
4015 Wilson Boulevard, Room 713
Arlington, VA 22203-1954

☐ Reprint (Orig + 2 copies) ☐ Technical Report (Orig + 2 copies)

☐ Manuscript (1 copy) ☒ Final Progress Report (Orig + 2 copies)

☐ Related Materials, Abstracts, Theses (1 copy)

CONTRACT/GRANT NUMBER: F49620-01-1-0484

REPORT TITLE: Experimental Characterization of Photonic Band Crystals for Tera Hertz Devices

SUBMITTED FOR PUBLICATION TO (applicable only if report is manuscript): N/A

Sincerely,

Dennis W. Prather, Associate Professor
University of Delaware
P: (302)-831-8170
F: (302)-831-8172
E: dprather@ee.udel.